ACS OMEGA

Open Access

http://pubs.acs.org/journal/acsodf

Article

Fabrication and Testing of Crop Waste *Ceiba pentandra* Shell Powder Reinforced Biodegradable Composite Films

Kaliraj Medadurai, Narayanasamy Pandiarajan,* Balavairavan Balasubramanian, and Balasundar Pandiarajan

Cite This: *ACS Omega* 2023, 8, 42762−42775

Read Online

ACCESS | Metrics & More | Article Recommendations

ABSTRACT: *Ceiba pentandra* shell powder (CPSP) biowaste is chosen as a biofiller combined with poly(vinyl alcohol) (PVA) as a matrix to make biofilms to increase the exploitation of biowaste materials and reduce the use of plastic materials. FTIR plots indicated no significant chemical reaction or formation of new functional groups during interaction between PVA and CPSP. XRD diffractograms showed that the crystallinity index (35.3, 38.6, 42.3, 46.4, and 48.5%) and crystalline size (18.14, 20.89, 23.23, 24.87, and 26.34 nm) of biofilms increased with CPSP loading (5−25 wt %). The PVA/CPSP films are thermally stable up to 322 °C. The peak highs of AFM images showed that the films' surface roughness gradually increased from 94.75 nm (5 wt % CPSP) to 320.17 nm (25 wt % CPSP). The FESEM micrographs clarify the homogeneous distribution of CPSP in the PVA matrix. Tensile strength and tensile modulus are noticeably increased by 26.32 and 37.92%, respectively, as a result of the loading of CPSP from 5 to 20 wt % in the PVA matrix. The PVA/CPSP films outperform pure PVA films in UV shielding (350−450 nm). The 59% weight loss of films was estimated during 60 days of burial. The fabricated biofilms maintained their suitable structural, thermal, morphological, and mechanical properties. Additionally, they exhibited consistent performance in ultraviolet (UV) barrier, opacity, water absorption, water vapor permeability, soil burial, and antimicrobial characteristics over time. Overall, PVA/CPSP (5−25 wt %) films are biodegradable and have promising applications as good packaging materials.

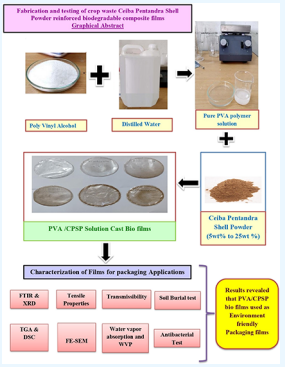

INTRODUCTION

Plastics are now becoming a core component for many applications such as automobiles, packaging, furniture, house appliances, etc. Because we produce and discard so many plastics, our necessity for plastic has another grave drawback.[1] In the 9 billion tonnes of plastic produced around the world as of 2010, 6.9 billion metric tons have been wasted, and just 9% have been recycled. The remaining plastic garbage is disposed of in landfills and waterways around the globe, where it causes pollution that harms species.[2,3] Ineffective packaging plastics comprise about 40% of the garbage. The development of environmentally friendly products has received a lot of attention recently, with ecofriendly materials being used as a probable replacement in lieu of plastic (derived from petroleum hydrocarbons) packaging materials.[4] The various benefits of biocomposite materials include their relative affordability, increased environmental friendliness, and inherent biodegradability.[5]

The production of biofilms with synthetic polymers that can provide high mechanical properties and are nonvenomous as an alternative to packaging plastics will be suitable for food packaging, biomedical, and enclosing applications.[6,7] In various fields, poly(vinyl alcohol) (PVA) is overtaking other nonbiological polymers like polyethylene, polypropylene, HDPE, etc., because it has the properties of biodegradability, nontoxicity, hydrophilicity, film-forming, and higher tensile strength.[8,9] Specifically, PVA is acknowledged as one of the most promising biodegradable polymers in mulch films.[10] PVA has some downsides, including a high degree of hydrophilicity due to PVA originating with more hydroxyl groups in its carbon chains and a sluggish decomposition rate in an anaerobic environment.[11] To improve the mechanical properties, biodegradation rate, and hydrophilic nature of PVA-based composites, combining them with organic fillers extracted from plant wastes may be viable.[12] Crop scum, farming rubbish, and byproducts are suitable biological reinforcement fillers for biocomposites.[13] Combining plant leftovers with polymeric materials results in a composite material with enhanced properties.

The Malvaceae tree family includes the genus *Ceiba* indigenous to tropical and subtropical regions of the Americas and tropical West Africa. The *Ceiba pentandra* (kapok) plant yields a strong and lightweight fiber used to stuff dolls, pillows,

Received: July 31, 2023
Revised: October 16, 2023
Accepted: October 19, 2023
Published: November 2, 2023

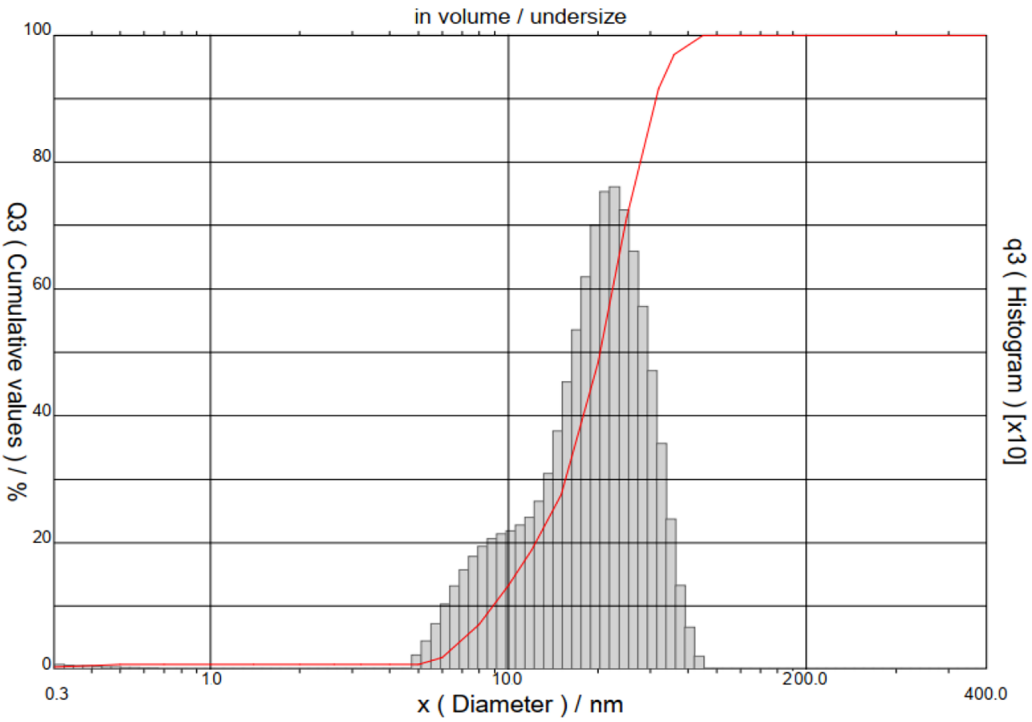

Figure 1. Particle size of *Ceiba pentandra* shell powder.

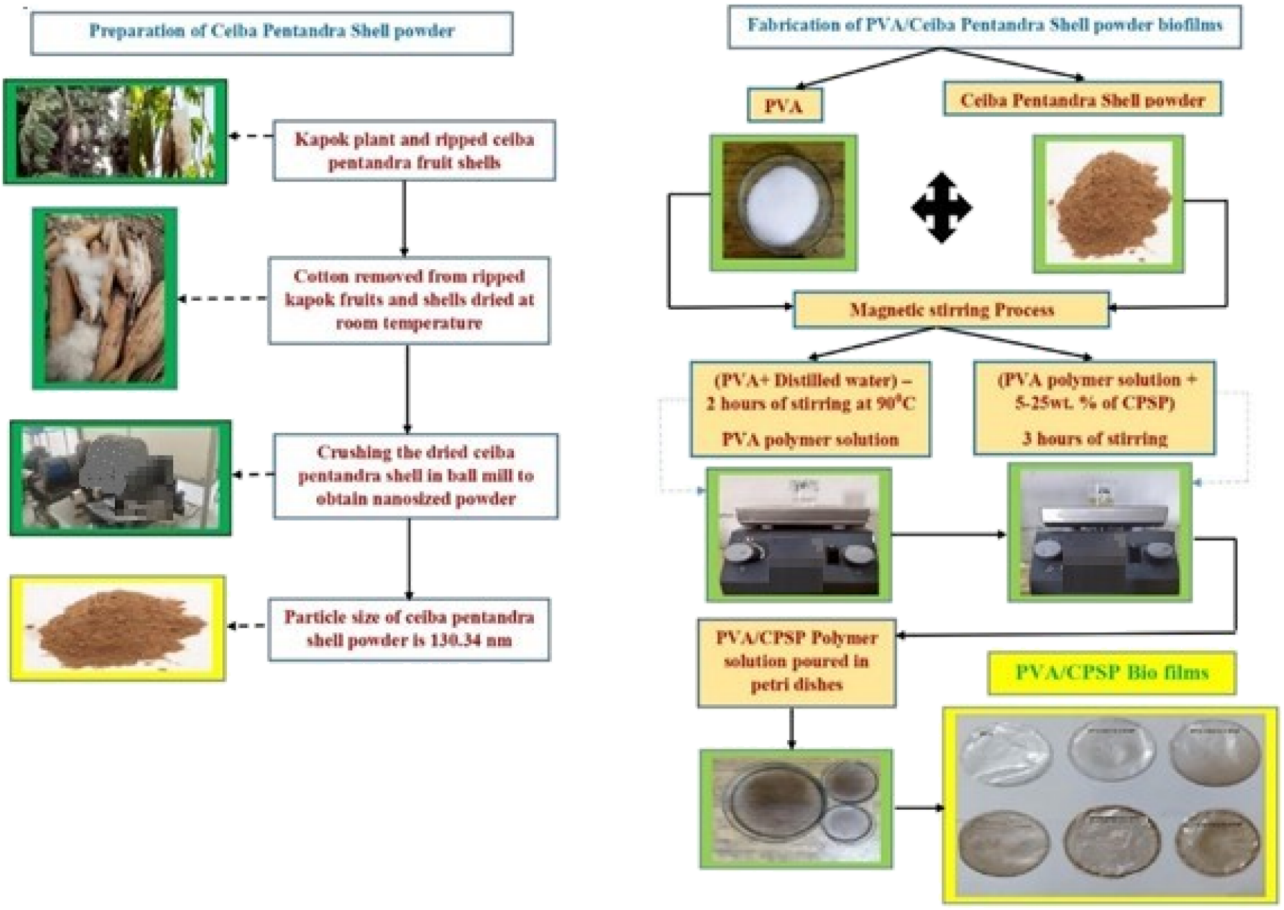

Figure 2. Preparation of *Ceiba pentandra* shell powder and PVA/CPSP biofilms.

mattresses, and tapestries.[14] The most prominent textile fiber is lint, produced from cotton, the king of natural fiber, collected from the torn *Ceiba pentandra* fruits.[15] Lint is the most comfortable and environmentally friendly textile fiber. Oils

https://doi.org/10.1021/acsomega.3c05577
ACS Omega 2023, 8, 42762−42775

used to prepare fertilizers and soap are extracted from the seeds of the *Ceiba* tree.[16] Because of their high fiber and tannin content, *Ceiba pentandra* seeds reportedly had a low feeding value. The outer shells of ripped *Ceiba pentandra* fruits are leathery, pendulous capsules 10−25 cm long and 3−6 cm in diameter. The mature fruit shells of *Ceiba pentandra* are underused and are more fibrous and biodegradable.[17] The bulk of the stalk is burned off in the fields after the cotton crop harvest.

In this particular context, a multitude of crops are identified and subsequently transformed into applications that are oriented toward industrial products. Currently, *Ceiba pentandra* fruit shells are predominantly burned off in the fields after cotton removal. The fruits ripen 80−100 days after flowering, and the shells of *Ceiba pentandra* fruit are highly fibrous, cellulosic, and porous in nature.[18] The primary aim of this research endeavor is to ascertain a novel economic biofiller material that can be utilized in the production of environmentally sustainable biocomposite films. A thorough analysis of the scientific literature indicated that the ripped fruit shell powder from *Ceiba pentandra* has not yet been documented as a reinforcement filler for PVA-based biofilms. This practice serves the purpose of reducing production costs and enhancing the overall properties of the biocomposite films.

In the framework, the objective of this work is to explore the effects of *Ceiba pentandra* shell powder content (5, 10, 15, 20, and 25 wt %) in PVA matrix on structural, mechanical, thermal, water resistance, UV-barrier, optical, biodegradable, and antimicrobial properties of the resultant biocomposite films. The biodegradation rate (% weight loss in soil) of PVA with NCSP, GBPF, and ZMCP fillers are 37.5, 42.5, and 57.5%, respectively, based on previous research articles. In this article, the fabricated PVA/CPSP biofilms exhibited 60.7% weight loss in soil. The information gained from this study will provide an excellent foundation for the practical uses of *Ceiba pentandra* ripped fruit shell powder, which may be appropriate for biobased packaging and enfolding materials.

Materials. Poly(vinyl alcohol) (PVA), 97% hydrolyzed (molecular weight of 120,000 and 1% ash max), and deionized water were obtained from Nice Chemicals (P) Ltd., Kochi, Kerala, India. PVA granules were white and kept in a sealed container. The ripped fruit shells were collected from a local cotton farm in Rajapalayam, Tamil Nadu, India. The cotton inside the ripped fruits of kapok was removed, and the outer shells were dried and crushed into nanosized reinforcement fillers. The average particle size of the *Ceiba pentandra* shell powder was 130.34 nm, measured by using microtrap optical particle size analyzers (Figure 1).

Fabrication of PVA/CPSP Biofilms

The preparation of *Ceiba pentandra* shell powder and PVA/CPSP biofilms is shown in Figure 2. The PVA/CPSP biofilms were made via the solution casting method. Twenty milliliters of deionized water was measured and poured into a beaker containing 2 g of hot water-soluble poly(vinyl alcohol) (PVA). Nearly 2 h of continuous magnetic stirring at 90 °C was employed to prepare the homogeneous PVA solution. The different proportions (5, 10, 15, 20, and 25 wt %) of CPSP were mixed with PVA solution and stirred for 2 h to get a consistent PVA/CPSP polymer solution. The mixture was then poured over the Petri dishes and allowed to dry for 12 h at room temperature. After that, films were demoisturized for 2 h at 50 °C in an oven. For each combination of PVA and the powdered *Ceiba pentandra* shell, five film samples were generated. The film, with an average thickness of 0.141 mm, was peeled off and desiccated for further characterization.

EXPERIMENTAL METHODS

Fourier-Transform Infrared Spectroscopy Analysis (FTIR). The functional group of samples (PVA matrix, *Ceiba pentandra* shell powder, and the PVA/CPSP bio composite films) was analyzed using Fourier transform infrared spectroscopy (RXI PerkinElmer). The film samples were reshaped into 10 × 10 mm for testing. The sample was placed on the base optic assembly, and the spectra were recorded. The characterization ranged from 4000 to 500 cm^{-1} in 45-time scanning to reduce noise and prevent spectrum overlapping at a resolution of 4 cm^{-1}.

X-ray Diffraction (XRD). An X-ray powder diffractometer analyzed the crystallinity and crystalline size of PVA, *Ceiba pentandra* shell powder, and fabricated PVA/CPSP biofilms. The intensity in the 2θ range from 6 to 40° at 4°/min obtained in the XRD (XPERT-PRO) was used to calculate the crystallinity index (CI) according to the following equation:[19]

$$\mathrm{CI} = \left[\frac{I_{200} - I_{100}}{I_{200}}\right] \times 100 \tag{1}$$

where I_{200} indicates the crystalline phase (2θ = 21−34°) and I_{100} indicates the amorphous phase (2θ = 17−20°)

The crystalline size of samples was calculated according to Scherrer's equation:[20]

$$\text{Crystallite size} = \left[\frac{k\lambda}{\beta \cos\theta}\right] \tag{2}$$

where k = Scherrer's constant (0.89), λ = wavelength of the radiation (0.1541 nm), and β = full width half-maximum (fwhm).

Atomic Force Microscopy (AFM). The surface roughness and structure observation of PVA/CPSP films was carried out by AFM model Park XE-70. The PVA/CPSP film samples were resized to 45 × 45 mm to measure their surface roughness. The test was conducted in a closed loop with a large area scanner XY > 90 μm, Z > 7.5 μm, and XY noise < 1.2 nm RMS, the typical imaging bandwidth. For PVA/CSPS film samples, the surface roughness parameters Ra, Rq, Rsk, and Rku were evaluated. Ra stands for average roughness, Rq for root-mean-square roughness, Rsk for skewness, and Rku for kurtosis.

TGA and DTG. Thermogravimetry analysis (TGA) and differential thermogravimetry (DTG) of PVA, *Ceiba pentandra* shell powder, and PVA/CPSP biofilms were executed using a thermogravimetric analyzer (TGA, NETZSCH STA 449F3-1100-M). Samples of about 2.5 mg kept in an alumina chamber were heated at 50−550 °C at a heating range of 10 °C/min under a nitrogen atmosphere.

Tensile Testing. Tensile strength, tensile modulus, and % elongation at break of the pure PVA and PVA/CPSP (5−25 wt %) biofilms were measured by a Universal Testing Machine (Instron 3369, ASTM D3039).[21] Five samples in each proportion of 100 × 10 mm were used. The machine specifications were as follows: machine speed, 100 mm/min; gauze length, 8 cm; and load, 500 N.

FESEM. The FESEM images of PVA, CPSP, and PVA/CPSP biofilms were obtained on a field emission scanning electron microscope (FESEM, Sigma HV, Carl Zeiss). The

https://doi.org/10.1021/acsomega.3c05577
ACS Omega 2023, 8, 42762−42775

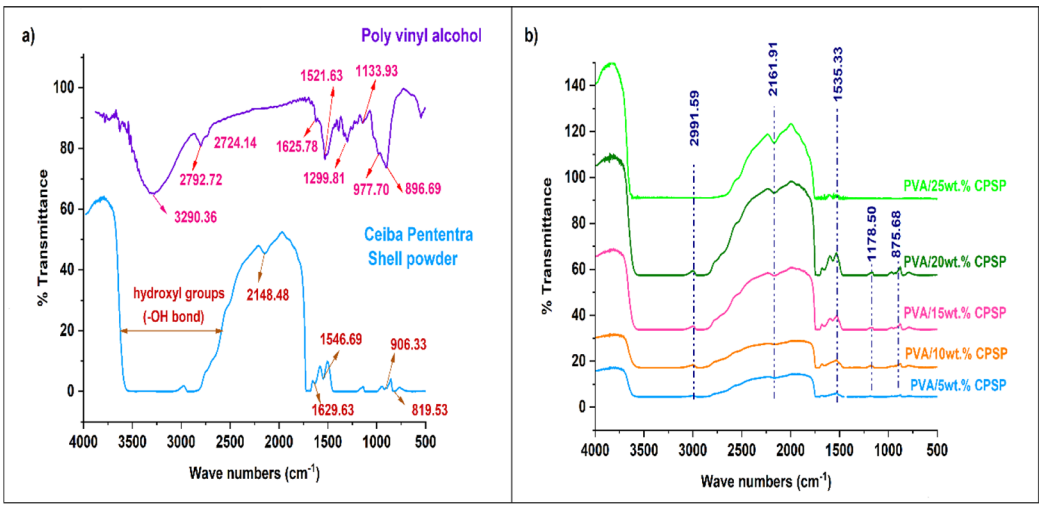

Figure 3. FTIR spectra of (a) pure PVA and *Ceiba pentandra* shell powder and (b) PVA/CPSP (5−25 wt %) biofilms.

experimental constraints were a resolution of 1000× magnification and an acceleration voltage of 20 kV. All film samples were cut into small pieces, which were then sputtered with gold to make the film samples conductive.

Ultraviolet−Visible (UV−Vis) Spectrograph. The transmittance of pure PVA and PVA/CPSP (5−25 wt %) biofilms was measured using an ultraviolet−visible spectrophotometer (Model 8451A, Hewlett-Packard Co., Santa Clara, CA, USA). The film samples were (30 × 30 mm) square shaped and measured in a series of wavelengths from 200 to 800 nm at a scanning rate of 200 nm/min.

The following equation calculated the opacity of the films:[22]

$$\text{Opacity} = [\text{absorbance at 600 nm}] \times [\text{film thickness}] \quad (3)$$

Water Intake. The % of water inhaled by the pure PVA and PVA/CPSP (5−25 wt %) biofilms was measured according to ASTM D570.[23,24] The 50 × 50 mm cross section of films was demoisturized in a vacuum oven at 50 °C for 24 h, chilled in a desiccator, and then promptly weighed (w_{dry}). The films were then completely soaked in distilled water at ambient temperature for the equilibrium test (24 h). The water on the film surface was detached after being removed from the container using a filter paper. Afterward, each film was weighed (w_{wet}). The % of water intake of the PVA/CPSP biofilm was calculated by using the following equation:

$$\text{Water intake} = \left[\frac{w_{dry} - w_{wet}}{w_{dry}}\right] \times 100\% \quad (4)$$

Water Vapor Permeability (WVP). The WVP of the PVA/CPSP biofilm was measured using the equipment and procedures outlined in ASTM E96 (ASTM, 1995). Before analysis, film samples were processed for 48 h in a chamber at 25 °C and 52% relative humidity. On cups with distilled water, films were placed and secured. In a desiccator cabinet that was kept at a controlled temperature and relative humidity, test cups were positioned.

The WVP was calculated from the slope (G) of a linear regression of weight loss versus time.

$$\text{WVP} = \frac{Gx}{A\Delta p} \quad (5)$$

where x is the film thickness, A is the area of the exposed film, and Δp is the differential water vapor partial pressure across the film.

Soil Burial Test. The indoor soil burial test explored the biodegradability of pure PVA and PVA/CPSP (5−25 wt %) biofilms using the methodology of Balavairavan et al. (2020).[25] Initially, the vacuum-dried sample weighed 0.62 g (Wi). Further, the film samples that had been vacuum-dried were buried separately in mud pots containing moist soil. The mud pots carrying the film samples (PVA and PVA/CPSP) were brooded at 23 °C for 2 months. Water was sprayed on the mud pots regularly to keep them damp. The film samples were taken from the mud pots once every 10 days to estimate the weight loss. The film samples were meticulously cleaned with water to remove the dust and then dried under a dryer until a constant weight (W_T) was achieved. The total % weight loss of film samples was calculated using the following equation:

$$\%\text{Weight loss of film} = \left[\frac{w_{initial} - w_{final}}{w_{initial}}\right] \times 100\% \quad (6)$$

where $w_{initial}$ is the initial weight and w_{final} is the final weight after 10 days.

Antimicrobial Activity. Antibacterial activity testing of pure PVA and PVA/CPSP films took place according to ASTM G 21-09 and prior investigations. Gram-negative *Escherichia coli* and Gram-positive *Salmonella* sp. microorganism were selected for bactericidal testing.

Statistical Analysis. Each property of the film was measured in five different places in individually prepared film samples, and the values were presented as mean ± standard deviation (SD).

RESULTS AND DELIBERATION

Fourier Transform Interferometry (FTIR). The spectra of PVA (Figure 3a) showed a broader peak at 3290.36 cm^{-1} owing to the stretching vibration of the hydroxyl group. The ranges of PVA showed a C−H stretching of aldehyde at 2792.72 and 2724.14 cm^{-1}. The stretching band found at 1625.78 cm^{-1} shows the C ═C group of alkenes. The peak at 1521.63 cm^{-1} is due to C−O carbonyl stretching, the peak at 1133.93 cm^{-1} is due of C−H bending vibration of CH_2, and the peak at 1133.93^{-1} is due to C−H deformation vibration.[25]

https://doi.org/10.1021/acsomega.3c05577
ACS Omega 2023, 8, 42762−42775

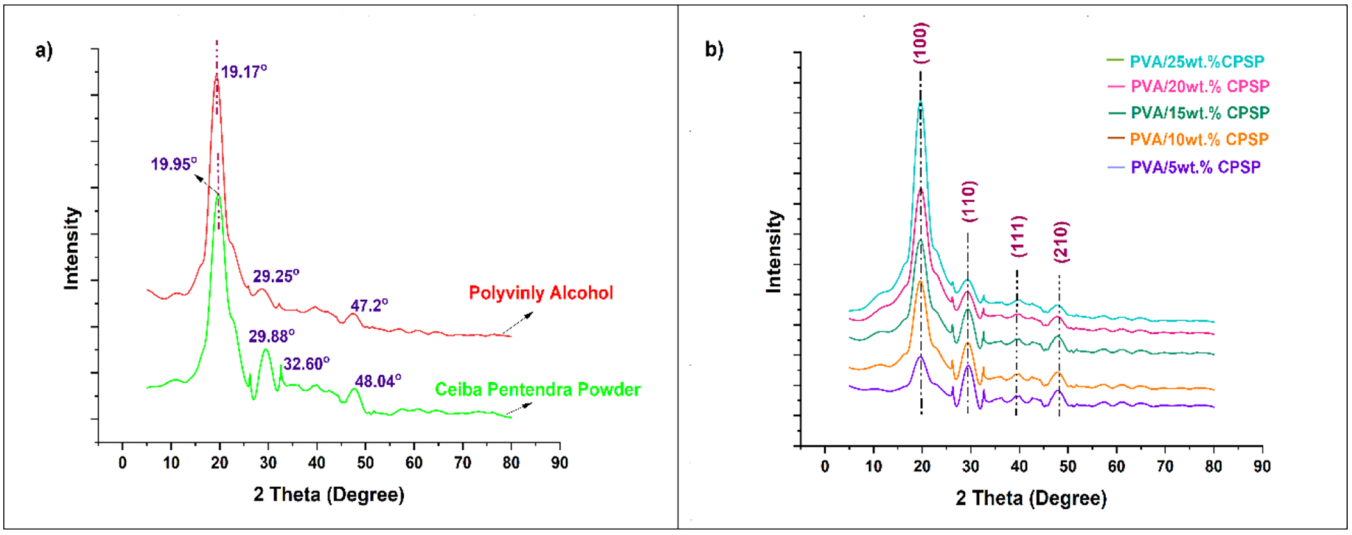

Figure 4. X-ray diffractograms of (a) pure PVA and *Ceiba pentandra* shell powder and (b) PVA/CPSP (5−25 wt %) biofilms.

The FTIR spectra of (Figure 3a) *Ceiba pentandra* shell powder showed the presence of −OH stretching (3400−3650 cm^{-1}), −CH stretching (2148.48 cm^{-1}), intermolecular hydrogen bonding (1629.63 cm^{-1}), and C═C stretching of cyclic alkene (819.56, 906.33, and 1546.69 cm^{-1}). As shown in Figure 3b, with increasing *Ceiba pentandra* shell powder, the peak at 3290.36 cm^{-1} (PVA) shifted to a higher wavenumber in the region of 3330 to 3560 cm^{-1} for all proportions of films. The lengthy flat peak of −OH bonds assimilated in all combinations of films is similar to the peaks of CPSP. This may be because CPSP and PVA form robust hydrogen bonds with one another. The characteristic peak of the C−H vibration from cellulose and hemicellulose was noticed in the infrared spectra at 2991.59 cm^{-1}. The peaks at 1652.99 and 1564.33 cm^{-1} reflected the aromatic C═C band, which merely occurs in lignin, showing that the lignin has been preserved in the shell particles of *Ceiba pentandra*. The 1178.50 cm^{-1} peak represented the bending of C−O stretching, a common peak for films containing CPSP up to 20 wt %. The peak at 1178.50 cm^{-1} vanished at the maximum filler material loading (25 wt %), and smooth IR spectra were seen. In PVA/CPSP films, the peak at 875.68 cm^{-1} is visible due to the C═C bending of alkane up to 20 wt % of filler; however, this peak also became extinct upon further CPSP loading. Overall, the good compatibility between PVA and CPSP is due to strong −OH bonding. In contrast to the peak patterns of PVA and CPSP, the PVA/CPSP biofilm did not show any significant band shifts or new peak patterns. This might result from the little chemical interaction between the constituent parts.

X-ray Diffraction (XRD). The X-ray diffraction test provides valuable data related to base materials' and film samples' degree of crystallinity and crystalline size. The X-ray outlines of PVA, CPSP, and PVA/CPSP films containing CPSP are shown in Figure 4a,b. X-ray diffraction patterns of the PVA displayed the scattering peak in the region from 2θ = 10 to 47.2° by the counts at 2θ = 19.17°. The *Ceiba pentandra* shell powder shows sharp peaks at 2θ = 19.95, 29.88, 32.60, and 48.04°, demonstrating that CPSP is I crystalline.

The PVA/CPSP film containing 5, 10, 15, 20, and 25% CPSP showed peaks with the counts at 2θ = 19.40, 19.83, 19.93, 20.01, and 19.81°, respectively. The XRD patterns of PVA/CPSP films revealed that all of the film samples are partly crystalline with a distinctive peak at 2θ = 20°. According to Aziz et al. (2020)[26] and Mori et al. (2020),[27] the XRD peak of PVA showed that the wide signal characteristic for the amorphous phase occurs at about 2θ = 19°. The XRD pattern of *Ceiba pentandra* shell powder indicated a high crystalline peak at 2θ = 19.95°. The crystallinity index and crystalline size of PVA, CPSP, and PVA/CPSP biofilms are shown in Table 1.

Table 1. Crystallinity Index and Crystalline Size of PVA, CPSP, and PVA/CPSP Biofilms

samples	crystallinity index (%)	crystalline size (nm)	physical nature
pure PVA	33.2%	17.34	semicrystalline
Ceiba pentandra shell powder	53.5%	32.34	crystalline
PVA/5 wt % CPSP	35.3%	18.14	semicrystalline
PVA/10 wt % CPSP	38.6%	20.89	semicrystalline
PVA/15 wt % CPSP	42.3%	23.23	semicrystalline
PVA/20 wt % CPSP	46.4%	24.87	semicrystalline
PVA/25 wt % CPSP	48.5%	26.34	semicrystalline

The crystallinity index of pure PVA has the lowest value compared to all of the film combinations. With the addition of CPSP filler (5−25 wt %), the crystallinity index of PVA/CPSP biofilms accelerated up to 27.12%; the increase in crystallinity index indicates that the physical structure of the biofilm has been enhanced and also that appropriate stress transfer occurred between the matrix to filler orientations. The increase in crystalline size corresponding to the addition of CPSP to the PVA matrix indicates that the surface roughness of biofilms increased and the resistance to deformation under external loads was also enhanced.

Atomic Force Microscopy (AFM). Atomic force microscopy can quantify the surface coarseness of samples down to the angstrom scale (0.1 nm).[28] To evaluate the topological features of the produced PVA/CPSP films, atomic force microscopy (AFM) was used. Phase contrast, histograms, roughness parameters, and 2D and 3D images were recorded. As seen in Figure 5a−e, the films exhibited both a smooth surface and some surface agglomerations at increasing wt % of CPSP, with a root mean square roughness (RMS) of a few nanometers. The agglomerated designs resemble separate

https://doi.org/10.1021/acsomega.3c05577
ACS Omega 2023, 8, 42762−42775

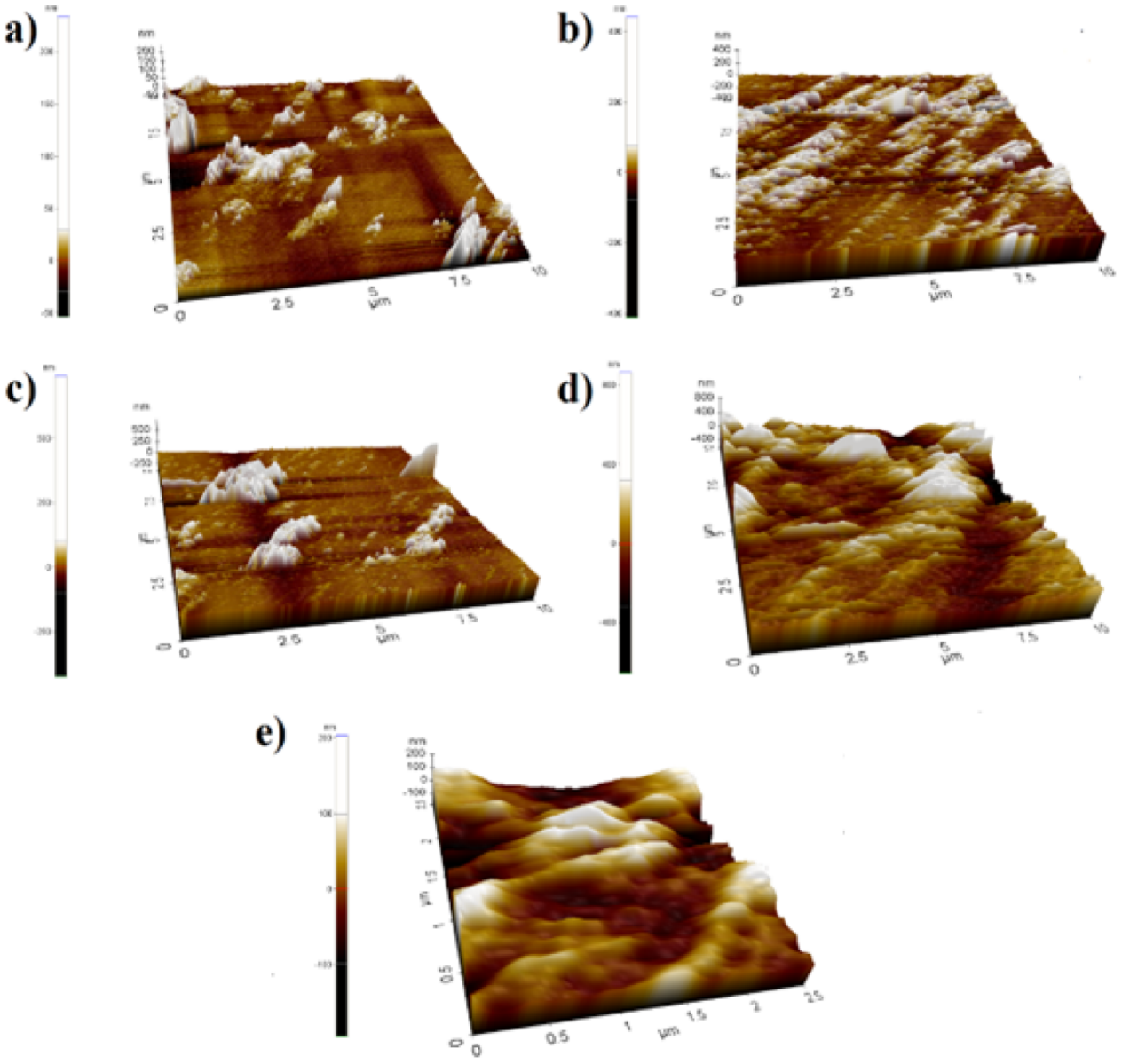

Figure 5. AFM micrographs of (a) PVA/5 wt % CPSP film, (b) PVA/10 wt % CPSP film, (c) PVA/15 wt % CPSP film, (d) PVA/20 wt % CPSP film, and (e) PVA/25 wt % CPSP film.

Table 2. AFM Parameters of PVA/CPSP (5−25 wt %) Biofilms

film sample	min (nm)	max (nm)	mid (nm)	mean (nm)	Rpv (nm)	Rq (nm)	Ra (nm)	RMS (nm)	Rsk	Rku
PVA/5 wt % CPSP	−25.75	68.99	21.61	0.00	94.75	16.98	11.04	83.75	−2.352	8.25
PVA/10 wt % CPSP	−29.08	78.46	24.68	0.00	107.55	18.37	12.11	93.71	−2.067	8.67
PVA/15 wt % CPSP	−61.23	138.14	38.45	0.00	199.38	29.48	30.62	141.8	−1.118	4.08
PVA/20 wt % CPSP	−76.59	161.06	42.23	0.00	237.65	38.94	21.02	161.4	−1.113	6.53
PVA/25 wt % CPSP	−86.82	233.35	73.26	0.00	320.17	72.50	52.91	252.5	−1.891	5.46

peaks, each measuring 1 μm in width and 80−260 nm in height. Particles in these structures range in size from 10 to 50 nm. The value of the phase contrast for all samples is about 5−10°, indicating good homogeneity and no phase separations up to 20% of CPSP in the PVA matrix. AFM parameters of PVA/CPSP (5−25 wt %) biofilms are listed in Table 2.

A low surface roughness, at about 20−25 nm, can be observed in the PVA film. Adding CPSP evidenced increased RMS to 82−84, 91−95, 138−142, 157−163, and 250−253 nm with increased CPSP contents of 5, 10, 15, 20, and 25 wt %, respectively, in the PVA matrix. This might be caused by CPSP's partial water insolubility; however, it can change the surface roughness at high concentrations in the PVA matrix.

TGA and DTG. To analyze the thermal stability and decomposition properties of films containing various concentrations (5−25 wt %) of *Ceiba pentandra* shell powder in a PVA matrix, thermogravimetric analysis was performed. TGA is a significant analysis used to examine the biofilm's thermal

https://doi.org/10.1021/acsomega.3c05577
ACS Omega 2023, 8, 42762−42775

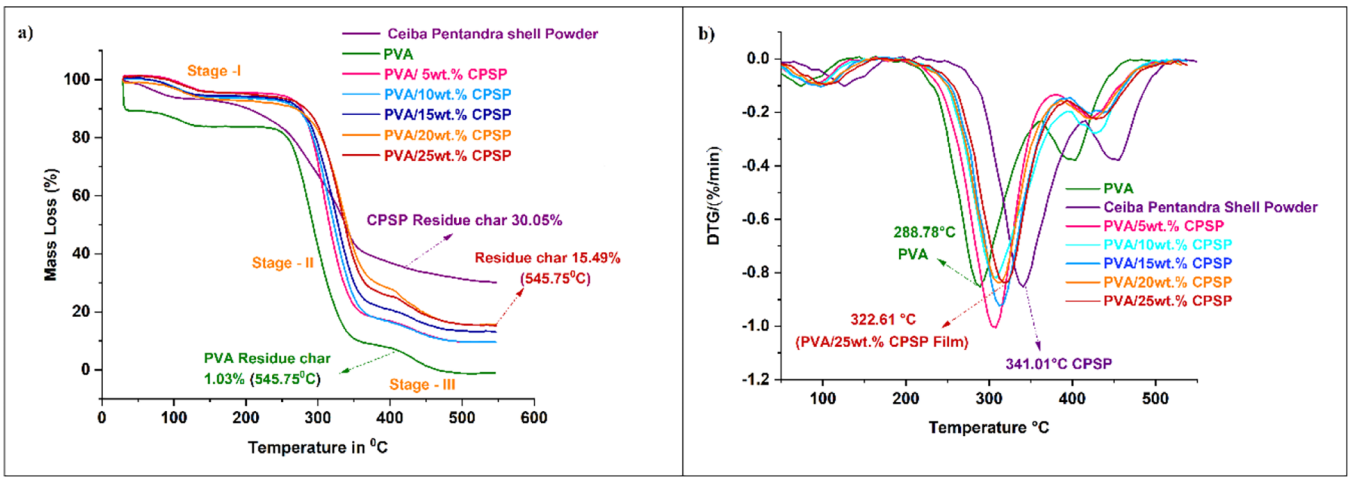

Figure 6. (a) Primary thermograms of PVA, CPSP, and PVA/CPSP biofilms. (b) Secondary thermograms of PVA, CPSP, and PVA/CPSP biofilms.

behavior and degradation. Figure 6a,bshows the thermogravimetric (TGA) and derivative thermogravimetric (DTG) curves of PVA, *Ceiba pentandra* shell powder, and PVA/CPSP (5−25 wt %) film samples. All curves followed a similar pattern, demonstrating that, for the PVA-based films, thermal degradation and mass loss ensued in three unique stages, each accompanied by a peak in the DTG curve that correlated to a distinct heating region. The initial thermal response induced the initial mass loss, which occurred below 100 °C. This was primarily because moisture and water vapor were eliminated.[29] Accordingly, PVA and PVA/CPSP films showed considerable weight loss compared to *Ceiba pentandra* shell powder. This observation is most likely explained by the high moisture content found across all combinations of test samples. Thus, the higher the moisture content is, the higher is the mass loss that arises in this phase. The second weight loss happened at temperatures between 150 and 290 °C after additional heating. The degradation of polymeric chains (cellulose and hemicellulose) and water residues was primarily responsible for this mass loss. Similar findings were previously reported by Yaradoddi et al.[30]

The film sample's final mass loss occurred at temperatures greater than 270 °C. The depolymerization and breakdown of the carbon chains in the PVA structure were responsible for the weight loss during this stage. From the data in Table 3, all films exhibited close decomposition temperatures that varied between 290 and 322 °C, higher than the controlled PVA's degradation temperature, which recorded its maximum decomposition at 288 °C, and less than the CPSP, which recorded its decomposition temperature at 341 °C. This evidence suggests that the incorporation of *Ceiba pentandra* shell powder enhanced the thermal stability of PVA/CPSP biofilm. Such results are consistent with the data obtained by Loganathan and Saravanakumar (2022),[36] who also studied the effect of orange peel powder on poly(vinyl alcohol) films and declared that the rate of degradation of films ranged from 290.9 to 295.4 °C.

Table 3. Maximum Degradation Temperature and % Residue for PVA, CPSP, and PVA/CPSP Biofilms

samples	degradation temperature (°C)	% residue at 545.75 °C
PVA	288.78	−1.03
Ceiba pentandra shell powder	341.01	30.05
PVA/5 wt % CPSP	308.04	9.57
PVA/10 wt % CPSP	309.22	9.61
PVA/15 wt % CPSP	312.39	13.07
PVA/20 wt % CPSP	317.61	15.23
PVA/25 wt % CPSP	322.61	15.49

Moreover, the thermal degradation of films was radically influenced by the addition of CPSP at various concentrations (5−25 wt %), representing the percentage of residue left after the final degradation, as shown in Table 4. Upon adding (5, 10, 15, 20, and 25 wt %) CPSP in PVA, the % residue increased by 9.23, 10.45, 12.43, 13.98, and 15.49%, respectively. This phenomenon demonstrated that, at temperatures above 320 °C, films with high concentrations of CPSP are more heat resistant than PVA films. These annotations aligned with previous studies by researchers investigating the effect of various cassava starch on PVA-based films and indicated that PVA/cassava starch films achieved thermal stability up to 300 °C.[31]

FESEM. FESEM micrographs of PVA, *Ceiba pentandra* shell powder, and PVA/CPSP biofilms are shown in Figure 7. FESEM plots (Figure 7a,b) of PVA and CPSP exhibited smooth and rough surfaces, respectively. The cross section of PVA films thickened after CPSP was added, as shown in Figure 7c−f, although all combinations of CPSP (5, 10, 15, and 20 wt %) in the film matrix seemed to be highly compatible. The incorporation of CPSP increased the coarser texture of PVA films, which is also confirmed by AFM analysis. The loadings of CPSP up to 20 wt % in the PVA matrix showed a smooth surface with no surface agglomerations. These results suggested that loadings of CPSP up to 20 wt % are well assimilated in the PVA film. Some agglomeration particles resulting from the inexorable phase separation were evident on the film surface. The agglomeration and voids observed at 25 wt % of CPSP may affect the tensile test parameters of PVA-based films (Figure 7g). Without significantly compromising the film homogeneity, blocking visible and UV light will be possible by incorporating *Ceiba pentandra* shell powder in PVA films.

Mechanical Properties. In particular, this study evaluates the tensile stress, Young's modulus, and % of elongation at break for pure PVA films and PVA/CPSP biofilms (5−25 wt %). Figure 8a shows that the tensile strength of the films

https://doi.org/10.1021/acsomega.3c05577
ACS Omega 2023, 8, 42762−42775

Table 4. Mechanical Properties and Thickness of Film Samples[a]

film samples	thickness of films in mm	tensile strength in MPa	Young's modulus in MPa	% of elongation at break
pure PVA	0.143 ± 0.03	13.72 ± 1.25	21.34 ± 0.95	50.3 ± 1.15
PVA/5 wt % CPSP	0.153 ± 0.0023	19.84 ± 2.01	35.58 ± 1.22	12.77 ± 0.95
PVA/10 wt % CPSP	0.158 ± 0.0012	24.95 ± 2.12	48.5 ± 1.56	9.39 ± 0.78
PVA/15 wt % CPSP	0.162 ± 0.034	28.81 ± 1.56	63.22 ± 1.05	6.14 ± 0.96
PVA/20 wt % CPSP	0.167 ± 0.024	29.93 ± 1.54	65.43 ± 1.34	5.15 ± 0.79
PVA/25 wt % CPSP	0.171 ± 0.045	26.95 ± 1.34	61.08 ± 1.44	6.32 ± 0.93

[a]Values are expressed as mean ± SD (n = 5).

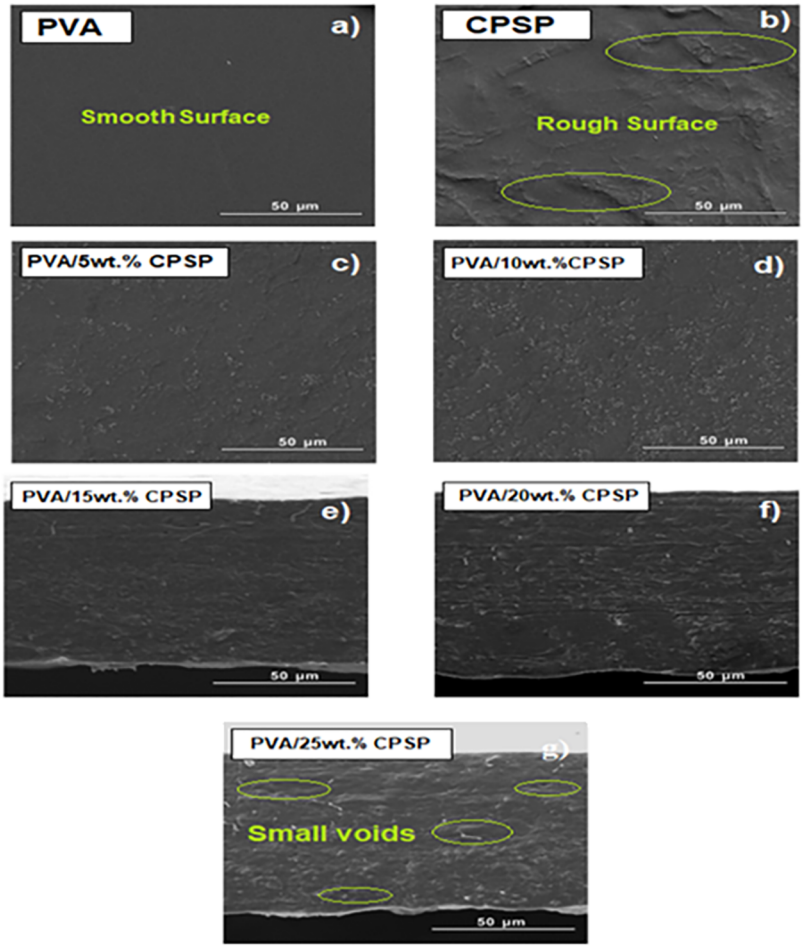

Figure 7. FESEM images of (a) PVA, (b) CPSP, (c) PVA/5 wt % CPSP, (d) PVA/10 wt % CPSP, (e) PVA/15 wt % CPSP, (f) PVA/20 wt % CPSP, and (g) PVA/25 wt % CPSP biofilms.

increased when the CPSP concentration was raised from 5 to 20 wt %. If the filler loading increased beyond 20 wt %, the transition stage was initiated, and the elongation of films increased because of poor compatibility between the matrix and filler. This result is consistent with a prior investigation made by Guimarães et al.[32] The PVA-based film with 20 wt % of CPSP showed the highest tensile stress (29.93 MPa), higher than that of films with 25 wt % CSPS (26.95 MPa) in the PVA matrix. The hydrogen bonds that formed between the molecules of PVA and CPSP are thought to be the cause of the high tensile stress at 20 wt % of CPSP content.[33] These bonds are primarily governed up to 20 wt % of CPSP and weaken when the concentration increases above 20 wt %. The maximum tensile strength (29.93 MPa) for PVA/20 wt % CPSP films in the current study was higher than that of PVA-based films with a mixing of 20 wt % of nano rice hull fillers (16.86 MPa). Similarly, that of PVA with 20 wt % of palm kernel shell powder obtained at 11 MPa is lower than the current study findings.

In essence, the stiffness of materials can be expressed by their Young's modulus (also known as their elastic modulus). It simply refers to how easily it can be stretched or bent. Figure 8a) shows that the effect of incorporation of *Ceiba pentandra* shell powder content (5−25 wt %) on the Young's modulus of PVA/CSPS films is the same compared with their corresponding tensile stress. The Young's modulus of PVA/CSPS films increased from 21.34 to 65.43 MPa for pure PVA film and PVA/20 wt % CPSP film, respectively. The stiffness of the films faintly diminished from 65.43 to 61.08 MPa as the concentration of *Ceiba pentandra* shell powder increased from 20 to 25 wt %. The better dispersion of CPSP up to 20 wt % improves their interaction with PVA matrices, thus leading to

https://doi.org/10.1021/acsomega.3c05577
ACS Omega 2023, 8, 42762−42775

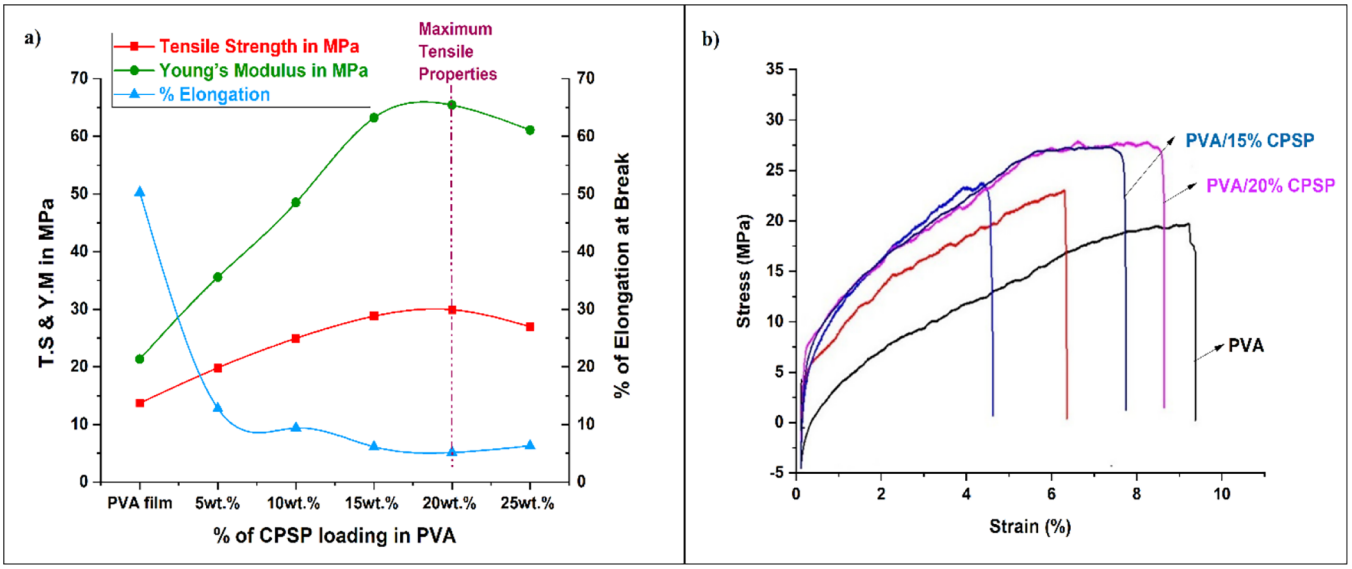

Figure 8. (a) Tensile properties of PVA and PVA/CPSP (5−25 wt %) biofilms. (b) Stress−strain curves of biofilms.

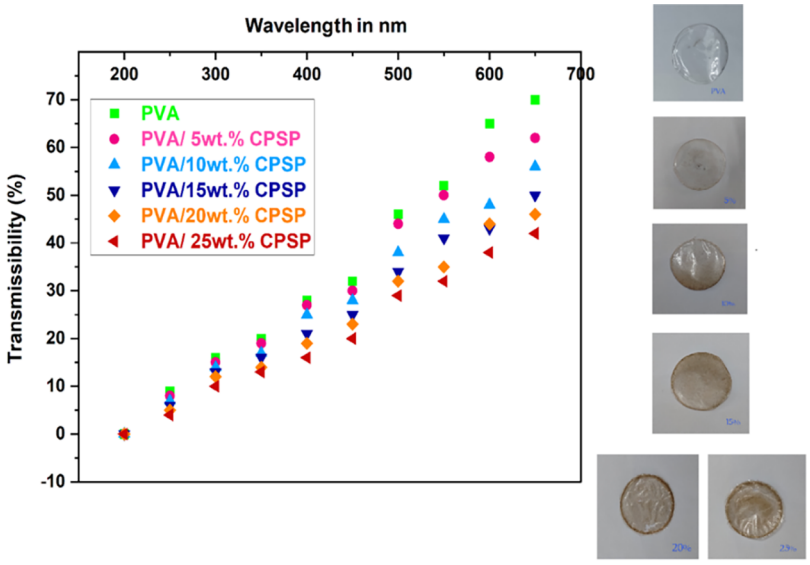

Figure 9. Transmissibility of pure PVA and PVA/ (5−25 wt % CPSP) biofilms.

the higher tensile strength and Young's modulus of PVA/CPSP biofilms. CPSP agglomeration appears to negatively impact tensile strength and Young's modulus, as evidenced by the higher surface roughness and lower tensile strengths of biofilms produced when the amount of CPSP is increased beyond 20 wt %.[34] Thus, Young's modulus of 25 wt % of CPSP-loaded films is reduced and then becomes less rigid. The elongation at break (EB) was found to be decreased to 50.3 (pure PVA film), 12.77, 9.39, 6.14, and 5.15% with the addition of 5−20 wt % of CPSP in the PVA matrix. The trend observed in the elongation at break in the study was similar to the loading of LASP[35] and green banana peel powder[36] with PVA described in previous studies. The mechanical properties and thicknesses of film samples are listed in Table 4. The type of fillers and polymer matrices, the concentration of fillers, the interfacial region, and the shape of the fillers can all impact the mechanical properties of polymers.[37]

UV-Light Barrier Properties. Effects of various concentrations of *Ceiba pentandra* shell powder (CPSP) content on the UV-light barrier property of PVA films are shown in Figure 9, and with the addition of CPSP, the transmittance of PVA films notably decreased at 200−800 nm wavelength. For the PVA films that were filled with 25 wt % of CPSP, film transmittance diminished from 70 to 35%. Moreover, the incorporation of 5−25 wt % of CPSP significantly increased the opacity (O) value, and transparency decreased. The PVA film with the highest content (25 wt %) of CPSP displayed the most significant O value, shown in Figure 10. The results proved that the light barrier capability of PVA films might be significantly increased by adding various amounts of CPSP particulate filler; when more CPSP is loaded, the PVA film can reveal a more vital light-blocking ability.

Various agrowaste particulate fillers were earlier used to improve the light barrier properties of packaging materials. Film transmittance in the UV and visible ranges decreased in PVA films strengthened with green banana peel powder.[37] A better film barrier quality was the principal outcome of the stuffing action of agrowaste particle fillers. Another inves-

https://doi.org/10.1021/acsomega.3c05577
ACS Omega 2023, 8, 42762−42775

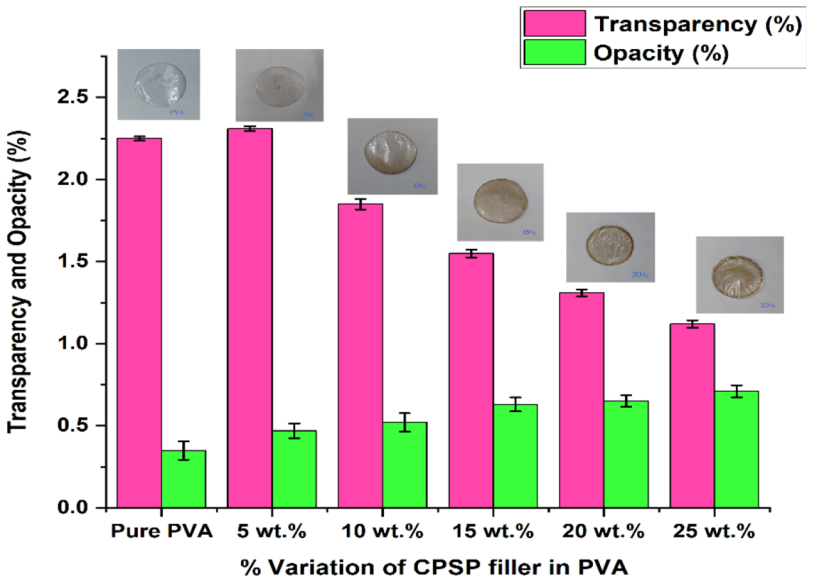

Figure 10. Transparency and opacity of pure PVA and PVA/CPSP biofilms.

tigation showed that incorporating the alkali-treated LASP[36] improved the opacity of a biopolymer-based film. The agglomeration of CPSP at higher loading proportions in the PVA matrix was primarily responsible for the decrease in transmittance at 800 nm and the increase in crystallinity generated by increasing the CPSP concentration in the film.

Water Absorption Test. The limitations of polymeric materials prohibit their widespread usage in numerous applications due to their high water absorption and solubility.[37] The water absorption properties of various PVA/CPSP film ratios were examined, and Figure 11 shows the % of water

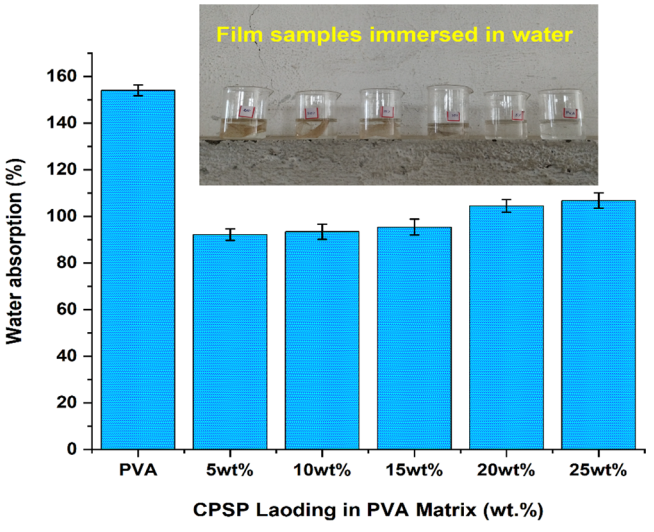

Figure 11. Percent water absorption of PVA and PVA/CPSP biofilms.

absorption over time. Figure 11 shows that adding *Ceiba pentandra* shell powder increases the PVA/CPSP film's water absorption %. This is because the hydrophilic *Ceiba pentandra* shell powder has a high fiber content and is easily influenced by water absorption. The water absorption capacity of the PVA/CPSP films with 5, 10, 15, 20, and 25 wt % of CPSP demonstrated an identical trend; however, the percentage of water absorption improves with the addition of CPSP content. All of the PVA/CPSP films tend to absorb water after being immersed in water for 5 h. The film lost its ability to absorb water after 300 min because it was saturated with water molecules.

Additionally, the PVA/CPSP films have the lowest percentage of water absorptivity among all combinations of films despite having the least amount of CPSP (5 wt %). This is because the *Ceiba pentandra* shell powder is not entirely enclosed by the PVA matrix, which makes the hydroxyl groups of PVA more readily available to water-binding sites. The absorption of water particles inside the films will be impeded by the zigzag path caused by an increase in the amount of CPSP in PVA. As equilibrium conditions were reached, the CPSP particles served as a stiff filler to lock the hydroxyl component interaction, causing the absorption of water by the films to reach saturation.[38]

Water Vapor Permeability (WVP). The WVP of poly(vinyl alcohol) films as a function of different concentrations (5−25 wt %) of CPSP is presented in Figure 12. As

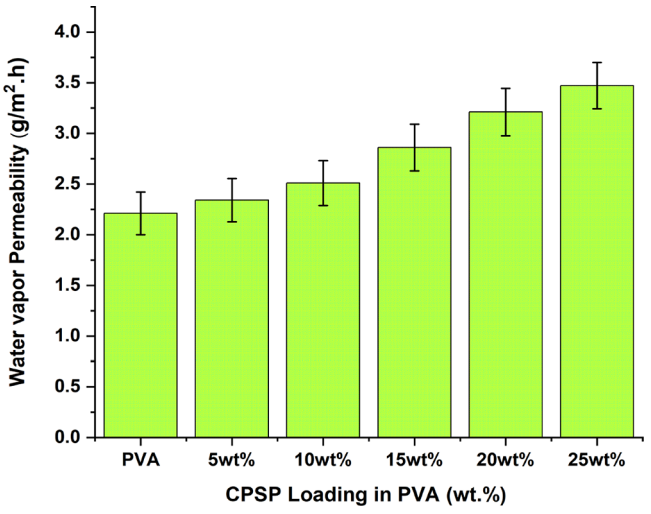

Figure 12. Percent water vapor permeability of PVA and PVA/CPSP biofilms.

https://doi.org/10.1021/acsomega.3c05577
ACS Omega 2023, 8, 42762−42775

can be seen, WVP increased linearly as the concentration of CPSP increased. These results could be related to structural modifications of the PVA network due to the incorporation of a highly fibrous filler and the hydrophilic character of *Ceiba pentandra* shell powder (CPSP), which favor the absorption and desorption of water molecules.[39] The highly fibrous plant waste filler CPSP causes greater flexibility in the polymeric structure, which increases the water sorbed mobility within the structure. As a result, WVP increases with the CPSP content.

Soil Burial Test. Biodegradability is a noteworthy property of packaging plastic materials. The seasonal conditions of the soil will provide a realistic environment for film degradation. The degradation occurs under the action of natural microorganisms (bacteria, fungi, etc.).[40] Figure 13 shows the indoor soil burial test chamber arrangement.

Figure 13. Indoor soil burial test setup.

The effect of *Ceiba pentandra* shell powder on the biodegradability of poly(vinyl alcohol) films was studied by evaluating the weight loss of the films under the soil burial condition. Figure 14 depicts the weight loss of controlled PVA films and films with various concentrations of CPSP after 2 months of burial in the soil. With an increase in the CPSP amount, the weight loss of all combination films increased significantly, which may imply that CPSP has a considerable impact on the biodegradability of the films. Additionally, tiny voids in films that absorb soil moisture are formed because of the high concentration of CPSP in PVA and reduced film density.[41] As stated in the results of the water intake study, the incorporation of CPSP from 5 to 25 wt % increased the hydrophilicity of the films with the hydroxyl groups bonded together. As a result, the water absorption of the PVA/CPSP films increased, which accelerated the decay of PVA/CPSP films.

According to the prior investigation, weight loss was similarly associated with the microbial deterioration of the films. The visually reviewed film samples reflected the weight reduction of all films perfectly (Figure 14).[42] In the soil burial test, the control PVA film lost roughly 30.2% of its original weight by the 60th day, but the PVA/5 wt % blend film lost 12.51% of its weight in only 20 days. By the 60th day, a significant weight reduction (44.5, 49.3, 52.4, 56.9, and 60.7%) was seen for PVA/CPSP films with 5, 10, 15, 20, and 25 wt % of CPSP.

Antimicrobial Test. To decrease the level of microbial growth in food, food packaging materials with antimicrobial characteristics are widely preferred. Hence, the antibacterial activities of the PVA and PVA/(5−25 wt %) of CPSP films against the microorganism *Salmonella* sp. and *Escherichia coli* were analyzed by measuring the diameter of the zone of inhibition. (Figure 15a,b, respectively). The antibacterial activity of different pathogens in film samples is shown in Table 5, which gives a clear indication of the antibacterial properties of PVA/CPSP biofilms.[43]

The neat PVA film was not found to have any antibacterial activity against the test organisms. However, CPSP-incorporated PVA films exhibited significant activity against both *Salmonella* sp. and *Escherichia coli*, thereby proving their applicability in protecting food from established pathogens. Consequently, *Ceiba pentandra* shell powder (CPSP), a high-fiber plant waste material, includes flavonoids and lipids that have the ability to suppress the growth of bacteria on PVA/CPSP biofilms, thereby providing a potential material for packaging.[44,45]

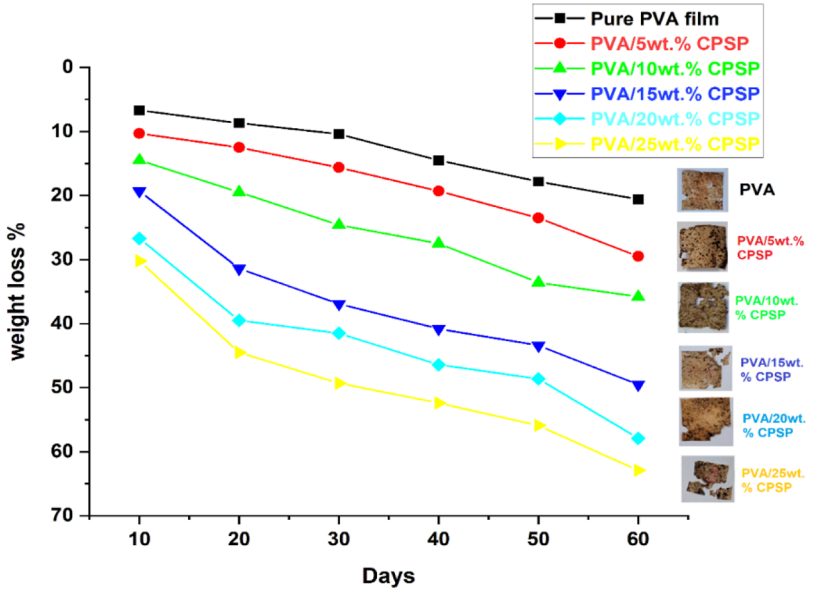

Figure 14. Percent weight loss of PVA and PVA/CPSP (5−25wt %) biofilms.

https://doi.org/10.1021/acsomega.3c05577
ACS Omega 2023, 8, 42762−42775

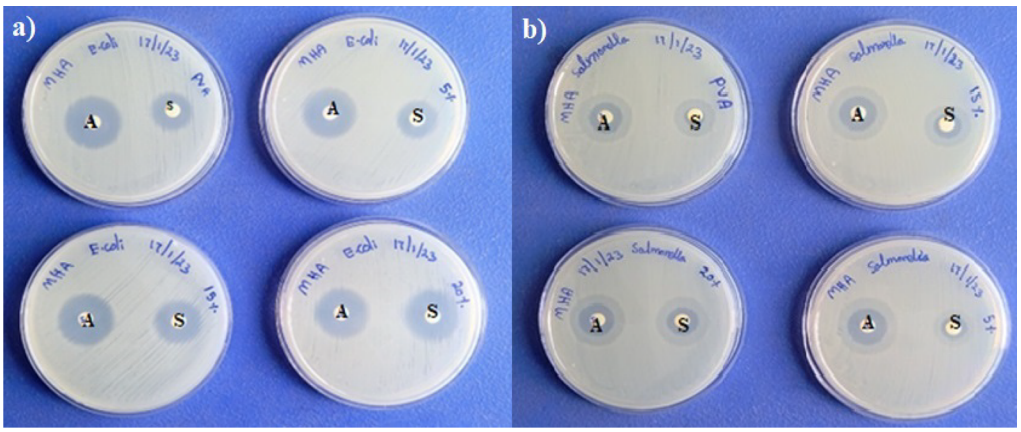

Figure 15. Antimicrobial activity of PVA and PVA/CSPS films against (a) *E. coli* and (b) *Salmonella* sp.

Table 5. Antibacterial Activity of Different Pathogens of PVA and PVA/CPSP Biofilms

		zone of inhibition in mm				
s. no.	organism	PVA	5%	15%	20%	25%
1	*Salmonella* sp.	8 mm	14 mm	12 mm	13 mm	11 mm
2	*Escherichia coli*	8 mm	9 mm	9 mm	10 mm	10 mm

CONCLUSIONS

Poly(vinyl alcohol) (PVA)−*Ceiba pentandra* shell powder (5, 10, 15, 20, and 25 wt %) biofilms were prepared using the solution casting method, and various tests characterized the films. The functional groups of PVA and CPSP interacted well according to FTIR spectra. The PVA/CPSP biofilms are semicrystalline, and the crystallinity of the biofilms at 25 wt % CPSP (48.5%) is comparatively higher than that of neat PVA (33.2%). Their thermal and mechanical properties influenced the high crystallinity of biofilms. At maximum loading of CPSP (25 wt %), the minor voids were only visible in the FESEM micrographs, indicating that the particles were evenly distributed and incorporated in the PVA matrix. The PVA/CPSP films were also observed to have increased light absorption against UV radiation. Consequently, the PVA/CPSP biofilms unveiled a substantial enhancement in tensile properties at appropriate loadings of CPSP (20 wt %). The PVA/CPSP films are suitable for applications with temperatures up to 320 °C. In addition, water absorption and WVP of films increased with increasing CPSP loading. The fact that both PVA and CPSP are water-sensitive and have hydroxyl groups in their chemical structures is considered to be the reason. Based on the soil burial test, the weight losses increased (up to 59% weight loss in 60 days) with increasing CPSP loading, indicating that the films can degrade faster. The antimicrobial activity of PVA/CPSP biofilms also increased with filler content against *Salmonella* spp. and *Escherichia coli* bacterial organisms. Hence, the experimental results suggest the potential of the PVA/CPSP biofilm to be used as a promising packaging film to ensure food safety.

AUTHOR INFORMATION

Corresponding Author

Narayanasamy Pandiarajan − *Department of Mechanical Engineering, Kamaraj College of Engineering and Technology, Madurai, Tamil Nadu 625701, India;* orcid.org/0000-0002-1436-8338; Email: narayananx5@gmail.com

Authors

Kaliraj Medadurai − *Department of Mechanical Engineering, AAA College of Engineering and Technology, Sivakasi, Tamil Nadu 625020, India;* orcid.org/0000-0002-9312-8948

Balavairavan Balasubramanian − *Department of Mechanical Engineering, Kamaraj College of Engineering and Technology, Madurai, Tamil Nadu 625701, India;* orcid.org/0000-0002-7646-2792

Balasundar Pandiarajan − *Department of Mechatronics Engineering, Kamaraj College of Engineering and Technology, Madurai, Tamil Nadu 625701, India;* orcid.org/0000-0002-3578-3733

Complete contact information is available at: https://pubs.acs.org/10.1021/acsomega.3c05577

Author Contributions

K.M. and N.P. conceived the research idea. K.M. fabricated the various proportions of PVA/CPSP biofilms. B.B. verified the analytical methods and test results. B.P. investigated the findings of this work. All authors discussed the results and contributed to the final manuscript.

Notes

The authors declare no competing financial interest.

REFERENCES

(1) Idumah, C.-I.; Obele, C.-M.; Ezeani, E.-O. Understanding interfacial dispersions in ecobenign polymer nano-biocomposites. *Poly-Plas Tech and Mater.* **2021**, *60* (3), 233−252.

(2) Skariyachan, S.; Manjunatha, V.; Sultana, S.; Jois, C.; Bai, V.; Vasist, K.-S. Novel bacterial consortia isolated from plastic garbage processing areas demonstrated enhanced degradation for low density polyethylene. *Environ. Sci. Pollut Res.* **2016**, *23* (18), 18307−18319.

(3) Aattache, A. Properties and durability of partially replaced cement-based composite mortars co-using powders of a nanosilica superplasticiser and finely ground plastic waste. *J. Build Eng.* **2022**, *51*, No. 104257.

(4) Asyraf, M.-R.-M.; Ishak, M.-R.; Sapuan, S.-M.; Yidris, N.; Ilyas, R.-A.; Rafidah, M.; Razman, M.-R. Potential application of green

https://doi.org/10.1021/acsomega.3c05577
ACS Omega 2023, 8, 42762−42775

composites for cross arm component in transmission tower: A brief review. *Int. J. Polym. Sci.* **2020**, *2020*, 1.
(5) Neto, J.; Queiroz, H.; Aguiar, R.; Lima, R.; Cavalcanti, D.; Doina Banea, M. A Review of Recent Advances in Hybrid Natural Fiber Reinforced Polymer Composites. *J. Renewable Mater.* **2022**, *10* (3), 561−589.
(6) Pan, Y.; Farmahini-Farahani, M.; O'Hearn, P.; Xiao, H.; Ocampo, H. An overview of bio-based polymers for packaging materials. *J. Bioresour. Bioprod.* **2016**, *1* (3), 106−113.
(7) Muneer, F.; Rasul, I.; Azeem, F.; Siddique, M.-H.; Zubair, M.; Nadeem, H. Microbial Polyhydroxyalkanoates (PHAs): Efficient Replacement of Synthetic Polymers. *J. Polym. Environ* **2020**, *28* (9), 2301−2323.
(8) Thong, C.-C.; Teo, D.-C.-L.; Ng, C.-K. Application of polyvinyl alcohol (PVA) in cement-based composite materials: A review of its engineering properties and microstructure behavior. *Constr Build Mater.* **2016**, *107*, 172−180.
(9) Mok, C.-F.; Ching, Y.-C.; Muhamad, F.; Abu Osman, N.-A.; Hai, N.-D.; Che Hassan, C.-R. Adsorption of Dyes Using Poly(vinyl alcohol) (PVA) and PVA-Based Polymer Composite Adsorbents: A Review. *J. Polym. Environ.* **2020**, *28* (3), 775−793.
(10) Sirivechphongkul, K.; Chiarasumran, N.; Saisriyoot, M.; Thanapimmetha, A.; Srinophakun, P.; Iamsaard, K.; Lin, Y.-T. Agri-Biodegradable Mulch Films Derived from Lignin in Empty Fruit Bunches. *Catal* **2022**, *12* (10), 1150.
(11) Banerjee, M.; Jain, A.; Mukherjee, G.-S. Microstructural and optical properties of polyvinyl alcohol/manganese chloride composite film. *Polym. Compos.* **2019**, *40* (S1), E765−E775.
(12) Gautam, S.; Sharma, B.; Jain, P. Green Natural Protein Isolate based composites and nanocomposites: A review. *Polym. Test.* **2021**, *99*, No. 106626.
(13) Sapuan, S.-M.; Harussani, M.-M.; Ismail, A.-H.; Zularifin Soh, N.-S.; Mohamad Azwardi, M.-I.; Siddiqui, V.-U. Development of nanocellulose fiber reinforced starch biopolymer composites: A review. *Phys. Sci. Rev. 21*, 2023, DOI: 10.1515/psr-2022-0007
(14) Baraniak, J.; Kania-Dobrowolska, M. Multi-Purpose Utilization of Kapok Fiber and Properties of Ceiba Pentandra Tree in Various Branches of Industry. *J. Nat. Fib.* **2023**, *20* (1), No. 2192542, DOI: 10.1080/15440478.2023.2192542.
(15) Patwardhan, S. B.; Pandit, S.; Ghosh, D.; Dhar, D. W.; Banerjee, S.; Joshi, S.; Gupta, P. K.; Lahiri, D.; Nag, M.; Ruokolainen, J.; Ray, R. R.; Kumar Kesari, K. concise review on the cultivation of microalgal biofilms for biofuel feedstock production. *Biomass Convers. Biorefin.* **2022**, *1*, 1−18.
(16) Silitonga, A.-S. Ceiba Pentandra: A Feasible Non-Edible Oil Source for Biodiesel Production. *Seeds* **2012**, *17* (24), 28−29.
(17) Liu, T.; Liang, R.; He, H.; Zeng, Y.; Hou, Z.; Liu, Y.; Yuan, J.; Luo, B.; Zhang, S.; Cai, C.; Wang, S.; Lu, D.; Nie, S. Nanocellulosic triboelectric materials with micro-mountain arrays for moisture-resisting wearable sensors. *Nano Energy* **2023**, *112*, No. 108480.
(18) Pratiwi, H.; Kusmono; Wildan, M. W. Oxidized Cellulose Nanocrystals from Durian Peel Waste by Ammonium Persulfate Oxidation. *ACS Omega* **2023**, *8* (33), 30262−30272.
(19) Daneshfozoun, S.; Abdullah, M.-A.; Abdullah, B. Preparation and characterization of magnetic biosorbent based on oil palm empty fruit bunch fibers, cellulose and Ceiba pentandra for heavy metal ions removal. *Ind. Crops Prod.* **2017**, *105*, 93−103.
(20) da Silva, C.-G.; Kano, F.-S.; dos Santos Rosa, D. Thermal stability of the PBAT biofilms with cellulose nanostructures/essential oils for active packaging. *J. Therm Anal Calorim.* **2019**, *138* (4), 2375−2386.
(21) Soeda, J.; Uemura, T.; Okamoto, T.; Mitsui, C.; Yamagishi, M.; Takeya, J. Inch-size solution-processed single-crystalline films of high-mobility organic semiconductors. *Appl. Phys. Express.* **2013**, *6* (7), No. 076503.
(22) Sisodia, R.; Jerry, K.; Pratim Das, P.; Gupta, P.; Gupta, S.; Chaudhary, V. Experimental study on mechanical behaviour of linen/epoxy and linen/hemp/epoxy hybrid polymer composite. *Mater. Today Proc.* **2023**, *78*, 372−377.
(23) Pagno, C. H.; Costa, T. M. H.; de Menezes, E. W.; Benvenutti, E. V.; Hertz, P. F.; Matte, C. R.; Tosati, J. V.; Monteiro, A. R.; Rios, A. O.; Flôres, S. H. Development of active biofilms of quinoa (Chenopodium quinoa W.) starch containing gold nanoparticles and evaluation of antimicrobial activity. *Food Chem.* **2015**, *173*, 755−762.
(24) Nor Arman, N.-S.; Chen, R.-S.; Ahmad, S. Review of state-of-the-art studies on the water absorption capacity of agricultural fiber-reinforced polymer composites for sustainable construction. *Constr Build Mater.* **2021**, *302*, No. 124174.
(25) Balavairavan, B.; Saravanakumar, S.-S.; Manikandan, K.-M. Physicochemical and Structural Properties of Green Biofilms from Poly (Vinyl alcohol)/Nano Coconut Shell Filler. *J. Nat. Fibers* **2020**, *18* (12), 2112−2126.
(26) Chhatariya, H.-F.; Srinivasan, S.; Choudhary, P.-M.; Begum, S.-S. Corn starch biofilm reinforced with orange peel powder: Characterization of physicochemical and mechanical properties. *Mater. Today Proc.* **2022**, *59*, 884−892.
(27) Aziz, S. B.; Marf, A. S.; Dannoun, E. M. A.; Brza, M. A.; Abdullah, R. M. The Study of the Degree of Crystallinity, Electrical Equivalent Circuit, and Dielectric Properties of Polyvinyl Alcohol (PVA)-Based Biopolymer Electrolytes. *Polymers* **2020**, *12* (10), 2184. Vol 12, Page 2184. 2020
(28) Mori, T.; Mori, T.; Fujii, A.; Saito, A.; Saomoto, H.; Kamada, K. Effect of Crystallinity in Stretched PVA Films on Triplet-Triplet Annihilation Photon Upconversion. *ACS Appl. Polym. Mater.* **2020**, *2* (4), 1422−1428.
(29) Parvej, M.-S.; Wang, X.; Fehrenbach, J.; Ulven, C.-A. Atomic force microscopy-based nanomechanical characterization of kenaf fiber. *J. Compos. Mater.* **2019**, *54* (15), 2065−2071.
(30) Yaradoddi, J. S.; Banapurmath, N. R.; Ganachari, S. V.; Soudagar, M. E. M.; Mubarak, N. M.; Hallad, S.; Hugar, S.; Fayaz, H. Biodegradable carboxymethyl cellulose based material for sustainable packaging application. *Sci. Rep.* **2020**, *10* (1), 1−13.
(31) Gisan, K.-A.; Chan, M.-Y.; Koay, S.-C. Solvent-cast Biofilm from Poly(lactic) Acid and Durian Husk Fiber: Tensile, Water Absorption, and Biodegradation Behaviors. *J. Nat. Fibers* **2020**, *19* (11), 4338−4349.
(32) Guimarães, M.; Botaro, V.-R.; Novack, K.-M.; Teixeira, F.-G.; Tonoli, G.-H.-D. High moisture strength of cassava starch/polyvinyl alcohol-compatible blends for the packaging and agricultural sectors. *J. Polym. Res.* **2015**, *22* (10), 1−18.
(33) Rahmadiawan, D.; Abral, H.; Railis, R. M.; Iby, I. C.; Mahardika, M.; Handayani, D.; Natrana, K. D.; Juliadmi, D.; Akbar, F. The Enhanced Moisture Absorption and Tensile Strength of PVA/Uncaria gambir Extract by Boric Acid as a Highly Moisture-Resistant, Anti-UV, and Strong Film for Food Packaging Applications. *J. Compos. Sci.* **2022**, *6* (11), 337.
(34) Zhao, D.; Feng, M.; Zhang, L.; He, B.; Chen, X.; Sun, J. Facile synthesis of self-healing and layered sodium alginate/polyacrylamide hydrogel promoted by dynamic hydrogen bond. *Carbohydr. Polym.* **2021**, *256*, No. 117580.
(35) Asadollahi, M.; Gerashi, E.; Zohrevand, M.; Zarei, M.; Sayedain, S. S.; Alizadeh, R.; Labbaf, S.; Atari, M. Improving mechanical properties and biocompatibility of 3D printed PLA by the addition of PEG and titanium particles, using a novel incorporation method. *Bioprinting* **2022**, *27*, No. e00228.
(36) Loganathan, L.; Saravanakumar, S.-S.; Murugan, R. Investigation of physico-mechanical, thermal, morphological, optical and biodegradation properties of polyvinyl alcohol films reinforced with alkali treated Limonia acidissima shell powder. *Polym. Compos.* **2022**, *43* (6), 3544−3559.
(37) Balavairavan, B.; Saravanakumar, S.-S. Characterization of Ecofriendly Poly (Vinyl Alcohol) and Green Banana Peel Filler (GBPF) Reinforced Bio-Films. *J. Polym. Environ.* **2021**, *29* (9), 2756−2771.
(38) Liu, Y.; Ahmed, S.; Sameen, D. E.; Wang, Y.; Lu, R.; Dai, J.; Li, S.; Qin, W. review of cellulose and its derivatives in biopolymer-based

for food packaging application. *Trends Food Sci. Technol.* **2021**, *112*, 532−546.
(39) Raj, V. A.; Sankar, K.; Narayanasamy, P.; Moorthy, I. G.; Sivakumar, N.; Rajaram, S. K.; Karuppiah, P.; Shaik, M. R.; Alwarthan, A.; Oh, T. H.; Shaik, B. Development and Characterization of Bio-Based Composite Films for Food Packing Applications Using Boiled Rice Water and Pistacia vera Shells. *Polymers* **2023**, *15*, 3456.
(40) Turan, D. Water Vapor Transport Properties of Polyurethane Films for Packaging of Respiring Foods. *Food Eng. Rev.* **2021**, *13* (1), 54−65.
(41) Urbanek, A.-K.; Rymowicz, W.; Mirończuk, A.-M. Degradation of plastics and plastic-degrading bacteria in cold marine habitats. *Appl. Microbiol. Biotechnol.* **2018**, *102* (18), 7669−7678.
(42) Yadav, J.; Chauhan, P. Recent Advances in Synthesis, Characterization, and Application of Nanotechnology in Wastewater Treatment- A Review. *Nanosci Nanotechnol. - Asia.* **2022**, *12* (3), 16 DOI: 10.2174/2210681212666220405162938.
(43) Shankar, S.; Teng, X.; Li, G.; Rhim, J.-W. Preparation, characterization, and antimicrobial activity of gelatin/ZnO nanocomposite films. *Food Hydrocoll.* **2015**, *45*, 264−271.
(44) Olewnik-Kruszkowska, E.; Gierszewska, M.; Jakubowska, E.; Tarach, I.; Sedlarik, V.; Pummerova, M. Antibacterial Films Based on PVA and PVA−Chitosan Modified with Poly(Hexamethylene Guanidine). *Polymer* **2019**, *11* (12), 2093.
(45) Huang, C.-L.; Lee, K.-M.; Liu, Z.-X.; Lai, R.-Y.; Chen, C.-K.; Chen, W.-C.; Hsu, J.-F. Antimicrobial Activity of Electrospun Polyvinyl Alcohol Nanofibers Filled with Poly[2-(tert-butylaminoethyl) Methacrylate]-Grafted Graphene Oxide Nanosheets. *Polymer* **2020**, *12* (7), 1449.

https://doi.org/10.1021/acsomega.3c05577
ACS Omega 2023, 8, 42762−42775